Received: 20 December 2021 | Revised: 10 March 2022 | Accepted: 14 April 2022

DOI: 10.1002/suco.202100901

ARTICLE

fib CEB-FIP WILEY

Extension of the *fib* MC 2010 for basic and drying shrinkage of alkali-activated slag concretes

Richard Caron[1,2] | **Ravi A. Patel**[1,2] | **Frank Dehn**[1,2]

[1]Institute of Building Materials and Concrete Structures (IMB), Karlsruhe Institute of Technology (KIT), Germany

[2]Materials Testing and Research Institute (MPA), Karlsruhe Institute of Technology (KIT), Germany

Correspondence
Richard Caron, Institute of Building Materials and Concrete Structures, Karlsruhe Institute of Technology (KIT); Materials Testing and Research Institute (MPA), Karlsruhe Institute of Technology (KIT), Germany.
Email: richard.caron@kit.edu

Funding information
Horizon 2020 Framework Programme, Grant/Award Number: 813596

Abstract

Alkali-activated slag is an alternative to ordinary Portland cement that has been studied for the past 20 years. One of the main challenges for its practical use is understanding and controlling its shrinkage behavior. In this study, new experimental results for two alkali-activated slag concrete mixes are presented under both sealed and unsealed conditions. The results show that basic shrinkage increases with increased sodium silicate ratio. Under unsealed conditions, the age to exposure to drying has a most significant impact on the final drying shrinkage. Finally, the mechanisms explaining shrinkage of such materials are discussed and the*fib* Model Code 2010 is extended for alkali-activated slag concrete using the new experimental results. The extended model consists of four parameters influencing the final values and the speed of both basic shrinkage and drying shrinkage. It is extensively compared with experimental datasets from the literature and improves significantly predictions compared with the original models for both basic and drying shrinkage. This demonstrates clearly the feasibility to extend it for predicting shrinkage of alkali-activated slag concrete.

KEYWORDS

alkali-activated slag concrete, *fib* model code 2010, shrinkage

1 | INTRODUCTION

Alkali-activated materials (AAMs) are alternatives to ordinary Portland cement (OPC) as binders for concrete. Slag is a by-product from the steel industry and is considered as one of the most promising precursors for AAMs. It hardens and gains reasonable compressive strength when it is mixed with alkali solutions, in particular sodium silicate (waterglass).[1] Alkali-activated slag (AAS) concrete presents a low permeability and a good resistance to chloride ingress.[2,3] The key challenges hindering the use of AAS include a quicker setting,[4,5] a faster carbonation,[6,7] and a higher shrinkage in comparison to OPC systems.[8] Nevertheless, both AAS and OPC systems can be regarded as poro-visco-elastic materials, with similar mechanical properties[9] and a comparable pore structure, the matrix of AAS though being denser.[10] The main reaction product of AAS is Calcium-Alumino-Silicate-Hydrate (C-A-S-H), which has similar properties as

Discussion on this paper must be submitted within two months of the print publication. The discussion will then be published in print, along with the authors' closure, if any, approximately nine months after the print publication.

Institute of Building Materials and Concrete Structures, Karlsruhe Institute of Technology (KIT), 76131 Germany

Calcium-Silicate-Hydrate (C-S-H) with more aluminum incorporation in the nano-structure. C-A-S-H is considered to be the key reaction product while considering shrinkage of AAS concrete.[11]

In the context of dimensional stability of concrete, creep and drying shrinkage are two important factors to be considered. Creep refers to deformations under sustained load, while drying shrinkage occurs due to the removal of moisture from concrete. The removal of moisture can occur under sealed conditions due to consumption of moisture during the reaction. Induced strain from this phenomenon is referred to as basic shrinkage. Both creep and drying shrinkage can build up complex stress states that can lead to cracking under restrained conditions.[8,12,13] This causes a reduction of mechanical performances and durability of the concrete. In practice, for OPC-cement-based concrete, creep- and shrinkage-induced strains are often predicted using engineering models such as ACI 209R-92,[14] the model of Bazant-Baweja B3,[15,16] the model from Gardner and Lockman GL2000,[17] CEB FIP models,[18–21] and the *Fédération internationale du béton (fib)* Model Code 2010.[22] The Bazant-Baweja B3 model has been further updated and extended for blended cements with fly ash and slag in the B4 model.[23,24] Both *fib* MC 2010 and B4 model propose creep and shrinkage predictions from the compressive strength. The advantage of the *fib* Model Code 2010 is that all input parameters are related to the compressive strength f_{cm}, the type of cement, and the curing conditions, which are readily available to engineers. It has been recently extended for recycled aggregate concrete.[25] Chen et al. adapted also the Eurocode 2, a modified model from CEB/FIP model, for Supplementary Cementitious Materials (SCM).[26]

Three main theories have been developed for OPC systems to explain shrinkage resulting from the removal of moisture in terms of physical mechanisms. The first one is the capillary pressure theory wherein concrete is regarded as a poro-elastic material. Shrinkage is due to the capillary pressure developing in its pores after the consumption of water from the chemical reaction of hydration.[27–31] The second one is the surface tension theory which focuses on the mechanical equilibrium of water molecules in a porous material.[32–35] The third one is the disjoining pressure theory. It is based on the idea of adsorbed water removal from the surfaces of the pore walls of the porous material.[36,37] More recently, a creep theory has emerged in which shrinkage is considered as the deformation due to the viscoelastic behavior of concrete caused by the load induced by the capillary pressure.[11,38]

The shrinkage mechanisms for AAS concrete remain still unclear. According to some authors,[10,39] higher shrinkage observed for AAS in comparison to OPC would be explained through the capillary pressure theory. The denser pore structure of AAS leads to a higher capillary pressure and correspondingly a higher shrinkage.[10] It was also stated that drying shrinkage and water loss were not directly correlated.[10,29] For Song et al.,[40] keeping a high internal relative humidity in the AAS matrix reduces the basic shrinkage, in accordance with the capillary pressure theory. Ye et al.[29] showed that when samples are dried at different relative humidity steps, the correlation between the imposed external relative humidity and the final shrinkage at each relative humidity is different for AAS than for OPC. For them, further mechanisms should occur like creep effects at high relative humidity or pore-collapse in the case of step-wise drying. As reported by Li et al.,[31] the capillary theory should not be the only mechanism explaining shrinkage: the reduction of the steric-hydration force and creep effects should be considered to predict basic shrinkage of AAS paste.

In the context of AAS concrete, only few studies measuring both basic and drying shrinkage are available.[41] Second, very few engineering model extensions exist and can be applied to AAS concrete. This contribution addresses both issues and presents new experimental results for two new AAS concrete mixes for both basic shrinkage and drying shrinkage. Using these experimental data, the applicability of the existing *fib* MC 2010 for AAS is evaluated and an approach to extend the *fib* MC 2010 for AAS concrete for both basic and drying shrinkage is presented. The model extension is rigorously tested against 23 different datasets available in the literature, many of which only provide information on total shrinkage.

TABLE 1 Chemical composition of the anhydrous slag

Oxide	CaO	SiO_2	Al_2O_3	MgO	Others
Mass (%)	38.8	36.3	12.8	8.0	4.1

2 | MATERIALS AND METHODS

In this section, details on the material and the mixes used for new experiments reported in this study are presented. This is followed by the experimental methods and used protocols.

2.1 | Materials

Two AAS concrete mixes were tested using the slag provided by Ecocem (Netherlands). The chemical composition of the slag was measured using energy dispersive x-ray fluorescence (XRF) M4 Tornado spectrometer

TABLE 2 Fresh concrete characteristics, compressive strength, and Young's modulus of the concretes

Mix		Mix lS	Mix hS
w/s	[kg/kg]	0.45	0.45
n	[Na_2O g/100 g slag]	5.0	5.0
M_S	[SiO_2/Na_2O mol/mol]	0.5	2.2
Precursor content	[kg/m^3 of concrete]	450	
Sand (0–2 mm)	[vol-%]	40	
Agg. (2–8 mm)	[vol-%]	30	
Agg. (8–16 mm)	[vol-%]	30	
Flow diameter	[cm]	50	65
Density	[kg/m^3]	2.25	2.32
Air content	[%]	1.60	1.60
f_{cm}	[MPa]	56	76
E_{ci}	[GPa]	32	30

(Bruker GmbH Karlsruhe, Germany) and is given in Table 1. This composition is in the range of CaO, SiO_2, Al_2O_3, and MgO content in comparison to what can be found in the literature.[42–46] The slag coefficient $\frac{CaO+MgO}{SiO_2}$, considered as the main parameter for slag oxide composition[47,48] is in the lower range in comparison to other mixes. Two sodium silicate solutions were used for activation of slag to obtain two different mixes. Both mixes had the same water-to-slag ratio w/s equal to 0.45 and the same alkalinity coefficient $n = 5.0$ [Na_2O g/100 g slag] but different sodium silicate ratios M_S [SiO_2/Na_2O mol/mol]. The mix with M_S equal to 0.5 was designated mix lS, while the mix with molar ratio 2.2 was designated mix hS. The concrete was cast with the same precursor content of 450 kg/m^3 of concrete.

The flow spread, the density, and the air content of the fresh concrete were tested following the norms DIN EN 12350-5,[49] DIN EN 12350-6,[50] and DIN EN 12350-7,[51] respectively. Characteristic compressive strength after 28 days was measured following the norms DIN EN 12390-3[52] with three cubes of nominal size 100 mm while the Young's modulus after 28 days was determined following the norm DIN EN 12390-13[53] (method B) on six cylinders of diameter 100 mm and height 285 mm. Both mix designs and their characteristics are summarized in Table 2. For these tests, the samples were covered with plastic foil until testing in a chamber at 20 °C.

2.2 | Methods

2.2.1 | Casting of samples

The alkali solutions were prepared 24 h before their first contact with the slag and the aggregates, so that the temperature of the solution was stabilized at the ambient temperature (20 °C). The casting procedure was the following: the slag, the sand, and the aggregates were first mixed together during half a minute. Then, the solution was added and the whole was mixed for a minute. After 30 s of resting, the concrete was mixed for 2 min. Cylinders of diameter 100 mm and height 285 mm were then filled. The specimens were demolded after 1 day and covered with plastic foils when the storage conditions required it. All the samples were stored at a temperature of 20 °C.

2.2.2 | Evolution of mechanical properties with time

The development of compressive strength and Young's modulus with time were determined with cylinders of diameter 100 mm and height 285 mm after 2, 7, 14, 28, and 56 days. The cylinders were covered with plastic foil and stored at 20°C until the test day. The norm DIN EN 12390-13[53] (method B) was followed for the determination of the Young's modulus. For each test day, three cylinders were used to first determine the compressive strength. Then, the Young's modulus was determined by loading three other cylinders at a loading equal to one-third of the compressive strength. These cylinders were then loaded until failure. Overall, the presented compressive strength was thus an average of six values for each test day. The shrinkage of the concrete was measured following the norm DIN EN 12390-16 [DIN EN 12390-16][54] with the same sample geometry. Measurements were carried out at least for 100 d. For both mixes, different storage conditions were investigated. Basic shrinkage was measured with covered specimens. Drying shrinkage was studied at a relative humidity of 65% with different

TABLE 3 Experimental plan for shrinkage tests

Name	Mix	t_s [d]	RH [%]
lS-BS	lS	n.a.	n.a.
lS-DS-1d	lS	1	65
lS-DS-7d	lS	7	65
lS-DS-28d	lS	28	65
lS-DS-RH-43%	lS	7	43
lS-DS-RH-85%	lS	7	85
hS-BS	hS	n.a.	n.a.
hS-DS-1d	hS	1	65
hS-DS-7d	hS	7	65
hS-DS-28d	hS	28	65

Note: n.a. stands for not applicable.

exposure ages to drying (1, 7 and 28 days). The following nomenclature was assigned to each test: XX-YY(−Zd) with XX the name of the mix (XX = lS or XX = hS), YY the curing condition (YY = BS for sealed conditions, YY = DS for drying conditions), and Z the exposure age, if applicable (Z = 1, 7, or 28). For the mix lS, two other sets of specimens were sealed during 7 d and then unsealed and stored in curing chambers, respectively, at RH of 43% and 85%. For these experiments, the assigned nomenclature was lS-DS-RH-43% and lS-DS-RH-85%, respectively. All the shrinkage tests are summarized in Table 3. Three specimens were used for replication of test results for each condition. The standard deviation of shrinkage measurements for each condition varied between 0.5% and 1.5%, except for the specimens exposed to drying after 1 day, for which the standard deviation was equal to 4% for the mix lS and 6% for the mix hS.

3 | EXISTING MODELS FOR STRENGTH DEVELOPMENT AND SHRINKAGE IN THE *FIB* MC 2010 AND ITS ADAPTATION TO AAS

In this section, the original models as proposed in the *fib* MC 2010 for both strength development and shrinkage are recalled. Then, the proposed extensions for these models are presented.

3.1 | Strength development with the *fib* MC 2010

The strength development of concrete as a function of time (t [days]) in the *fib* MC 2010 is modeled using the 28 days compressive strength f_{cm}:

TABLE 4 Coefficient s for different types of precursor to determine the strength development

f_{cm} [MPa]	Strength class of cement	s
≤ 60 MPa	32.5 N	0.38
≤60 MPa	32.5 R, 42.5 N	0.25
≤60 MPa	42.5 R, 52.5 N, 52.5 R	0.20
60	All classes	0.20

$$f_{cm}(t) = \beta_{cc}(t) \cdot f_{cm}(t=28) \tag{1}$$

with,

$$\beta_{cc} = exp\left[s\left(1 - \left(\frac{28}{t}\right)^{0.5}\right)\right] \tag{2}$$

where s is the coefficient characteristic to the strength class of the binder (given in Table 4). Similarly, the development of the Young's modulus ($E_{ci}(t)$) with time is predicted from the value of the Young's modulus at 28 days $E_{ci}(t=28)$:

$$E_{ci}(t) = \beta_E(t) \cdot E_{ci}(t=28) \tag{3}$$

where,

$$\beta_E = [\beta_{cc}(t)]^{0.5} \tag{4}$$

3.2 | Shrinkage modeling with the *fib* MC 2010

The total shrinkage $\varepsilon_{cs}(t)$ is the sum of both basic shrinkage $\varepsilon_{cbs}(t)$ and drying shrinkage $\varepsilon_{cds}(t,t_s)$:

$$\varepsilon_{cs}(t) = \varepsilon_{cbs}(t) + \varepsilon_{cds}(t,t_s) \tag{5}$$

where t is the concrete age in days and t_s is the concrete age in days at the beginning of drying. The basic shrinkage is calculated with:

$$\varepsilon_{cbs}(t) = \varepsilon_{cbs0}(f_{cm}) \cdot \beta_{bs}(t) \tag{6}$$

where,

$$\varepsilon_{cbs0}(f_{cm}) = -\alpha_{bs}\left(\frac{0.1 \cdot f_{cm}}{6 + 0.1 \cdot f_{cm}}\right)^{2.5} \cdot 10^{-6} \tag{7}$$

and

TABLE 5 Coefficient α_{bs}, α_{ds1} and α_{ds2} for different types of cement

Strength class of cement	α_{bs}	α_{ds1}	α_{ds2}
32.5 N	800	3	0.013
32.5 R, 42.5 N	700	4	0.012
42.5 R, 52.5 N, 52.5 R	600	6	0.012

$$\beta_{bs}(t) = 1 - exp\left(-0.2 \cdot \sqrt{t}\right) \tag{8}$$

where f_{cm} is the mean compressive strength at the age of 28 days, α_{bs} is a coefficient dependent on the type of cement (see Table 5).

The drying shrinkage can be predicted with:

$$\varepsilon_{cds}(t) = \varepsilon_{cds0}(f_{cm}) \cdot \beta_{RH}(RH) \cdot \beta_{ds}(t - t_s) \tag{9}$$

where

$$\varepsilon_{cds0}(f_{cm}) = [(220 + 110 \cdot \alpha_{ds1}) \cdot exp(-\alpha_{ds2} \cdot f_{cm})] \cdot 10^{-6} \tag{10}$$

$$\beta_{RH}(RH) = \begin{cases} -1.55 \cdot \left[1 - \left(\frac{RH}{100}\right)^3\right] & \text{for } 40 \le RH \le 99\% \cdot \beta_{s1} \\ 0.25 & \text{for } RH \ge 99\% \cdot \beta_{s1} \end{cases} \tag{11}$$

$$\beta_{ds}(t - t_s) = \left(\frac{(t - t_s)}{0.035 \cdot h^2 + (t - t_s)}\right)^{0.5} \tag{12}$$

$$\beta_{s1} = \left(\frac{35}{fcm}\right)^{0.1} \le 1.0 \tag{13}$$

RH is the relative humidity of the ambient atmosphere, h is the notional size of the specimen, and α_{ds1}, α_{ds2} are dependent on the type of cement (see Table 5).

3.3 | Adaptation of the *fib* MC 2010 to alkali-activated slag concrete

The *fib* MC 2010 models described above are applicable for OPC-cement-based concrete. In order to extend it to AAS concrete, the same approach as that proposed by Tosic et al.[25] for the shrinkage of recycled aggregate concrete is applied. The Equations (5), (8), and (12) are adapted with four new coefficients, ξ_{cbs1}, ξ_{cbs2}, ξ_{cds1}, and ξ_{cds2}:

$$\varepsilon_{cs}(t, t_s) = \xi_{cbs1} \cdot \varepsilon_{cbs}(t) + \xi_{cds1} \cdot \varepsilon_{cds}(t, t_s) \tag{14}$$

$$\beta_{bs}(t) = 1 - exp\left(-0.2 \cdot \xi_{cbs2} \cdot \sqrt{t}\right) \tag{15}$$

$$\beta_{ds}(t - t_s) = \left(\frac{(t - t_s)}{0.035 \cdot \xi_{cds2} \cdot h^2 + (t - t_s)}\right)^{0.5} \tag{16}$$

If the four introduced coefficients are equal to 1, Equations (14), (15), and (16) correspond to Equation (5), (8), and (12) from the original *fib* MC 2010. The term $\xi_{cbs1}\varepsilon_{cbs0}(f_{cm})$ can be seen as the final basic shrinkage of the material. This implies that a higher ξ_{cbs1} results in a larger final basic shrinkage. Likewise, $\xi_{cds1}\varepsilon_{cds0}(f_{cm}) \cdot \beta_{RH}(RH)$ can be regarded as the final drying shrinkage of the material and thus an increase in ξ_{cds1} leads to an increase in the final drying shrinkage.

ξ_{cbs2} and ξ_{cds2} are related to the speed of basic and drying shrinkage, respectively. If ξ_{cbs2} is greater than 1, the basic shrinkage is faster than the one predicted by the *fib* MC 2010 for OPC concrete. If ξ_{cds2} is lower than 1, the drying shrinkage is faster than the one predicted by the *fib* MC 2010 for OPC concrete.

In literature, higher shrinkage has been reported for AAS with waterglass when compared with OPC for paste, mortar, and concrete samples. For paste with n = 4.7 g Na_2O/100 g slag and M_S = 1.5 mol/mol, Li et al.[55] found that the basic shrinkage of the activated slag was around 14 times higher after 7 days than the one for cement. For mortar, the basic shrinkage was found to be four to six times higher after 6 months than cement.[30,40,56,57] The results from Ballekere Kumarappa et al.[30] suggested that a higher n or a higher M_S result in a higher basic shrinkage. Still for mortars, the total shrinkage after 6 months of AAS was measured between 1.5 and 7 times higher than for cement for different ambient relative humidity conditions.[56–60] The results from Atis et al.[58] also indicated that a higher n resulted in more shrinkage, and that an increase of M_S also drastically increased the shrinkage. Ye et al.[61] showed that the total shrinkage of AAS was between 1.5 and 2 times higher after 25 days for mortars with a drying exposure age equal to 7 days. For concrete samples, drying and total shrinkage were found to be between 1.5 and 3 times higher after 2 months for AAS with waterglass than for OPC.[10,62,63] Shrinkage as a function of n and M_S was studied by Taghvayi et al.[63] on the concrete level. Their conclusions were in line with that of Ballekere Kumarappa et al.[30] and Atis et al.[58] that M_S had a much larger effect on shrinkage than n. Note that Taghvayi et al.[63] did not distinguish basic shrinkage and drying shrinkage with the convention from the *fib* MC 2010. For this reason, the relative importance of both types of shrinkage could not be assessed from their results.

The Equations (14), (15), and (16) were calibrated on experimental results obtained in this study. The

parameters ξ_{cbs1} and ξ_{cbs2} were calibrated with the results of basic shrinkage, while ξ_{cds1} and ξ_{cds2} were calibrated with the results of drying shrinkage. The calibration was done with the least squares method on the average values of the measured shrinkage. The optimization for the basic (resp. drying) shrinkage was done with the following objective function:

$$\mathcal{F}_{obj}(\xi_1,\xi_2,t_0) = \omega_1 \cdot \left(\mathcal{F}^{model}(\xi_1,\xi_2,t \le t_0) - \mathcal{F}^{exp}(t \le t_0)\right)^2 + \omega_2 \cdot \left(\mathcal{F}^{model}(\xi_1,\xi_2,t > t_0) - \mathcal{F}^{exp}(t > t_0)\right)^2 \quad (17)$$

for which $\mathcal{F}^{model}$ is the model function for basic (resp. drying) shrinkage, $\mathcal{F}^{exp}$ is the corresponding experimental data, $\xi_1 = \xi_{cbs1}$ (resp. ξ_{cds1}) and $\xi_2 = \xi_{cbs2}$ (resp. ξ_{cds2}). ω_1 is the weight affected to the early-age part of the curve, ω_2 the weight affected to the late-age part of the curve, and t_0 the shifting time chosen arbitrarily between early-age and late-age. By definition, $\omega_1 + \omega_2 = 1$. Studying the optimization with different objective functions, that is, different weights and shifting times allows the evaluation of the sensitivity of the obtained results with potential biases due to the difference of amount of data for early and late age. The optimization done with the same dataset but with different values of weights and shifting times showed that the obtained model parameters varied at most by 15% for ω_1 in range of [0.15, 0.6], ω_2 in range of [0.4,0.85], and t_0 in range of [10 d, 50 d]. Based on this sensitivity analysis, the model parameters reported in this study are that obtained when the function $\xi_{cbs1} \cdot \varepsilon_{cbs}(t \le t_0, \xi_{cbs2})$ (resp. $\xi_{cds1} \cdot \varepsilon_{cds}(t \le t_0, \xi_{cds2})$) is directly optimized on the experimental results using the simplified objective function with ω_1 equal to 1, ω_2 equal to 0, and $t_0 \to \infty$ in Equation (17). In order to ensure that the optimized parameters correspond to the global minimum and not to a local minimum, the optimization was carried out with different initial guesses that always resulted in the same model parameters.

It should be noted that the comparison between shrinkage values and the adapted *fib* MC 2010 model for AAS concrete should be made with caution. Indeed, for this model the role of final shrinkage value (both basic and drying) is primordial. Nevertheless, shrinkage rates of the experiments led in this study seem to be stabilized, and the extrapolated final values should be in the good range of the final true values. For AAS concrete, only few results are available for long term. The results from Collins et al.[10] indicated that the speed of shrinkage was not very affected by the used precursor and thus the results can be compared directly in terms of amplitude.

4 | RESULTS

In this section, the experimental results are presented and discussed. This is followed by comparing them to existing models from the *fib* MC 2010. The evaluation of the parameters for the model extensions are also presented in Sections 4.2.2 and 4.2.3.

4.1 | Experimental results

4.1.1 | Strength development

The evolution of measured compressive strength and Young's modulus on sealed cylinders are given in Figure 1. After 7 days, the mixes lS and hS attained 76% and 75%, respectively, of the compressive strength after 28 days. The Young's modulus development is faster than the compressive strength development with values at 7 days equal to 91% and 93% of that at 28 days for the mixes lS and hS, respectively.

4.1.2 | Basic shrinkage

The experimental results for the basic shrinkage of the two mixes are shown in Figure 2. The basic shrinkage of the mix hS is around two times higher than the one of the mix lS. Thus, the increased amount of silicon in the alkali solution induces a higher shrinkage. Such a result is in accordance with study done by Ballekere Kumarappa et al.[30] for mortars. After 50 days, the further shrinkage evolution of the mix hS is very low (99% of final shrinkage achieved within 50 days) when compared with the mix lS.

In comparison to OPC, AAS has a finer pore structure.[10] This leads to a larger capillary pressure and thus to a larger shrinkage due to the self-desiccation, as postulated previously by different researchers.[10,27,28] Chemical shrinkage also contributes significantly to explain basic shrinkage. It refers to the fact that, as reaction products are smaller than the reactants, internal voids are generated in the matrix. These voids are the primary cause of the formation of the meniscus in the pore structure that lead to the development of the capillary pressure. Cartwright et al.[64] showed that the chemical shrinkage of AAS is lower than for cement. For Li et al.,[31] the measured chemical shrinkage of AAS is equal to the one of OPC. Models from Ye et al.[65] and Thomas et al.[66] predict that the chemical shrinkage is above 12 mL/100 g slag, two times higher than the chemical shrinkage of Portland cement.[67] In all, there is no consensus on the relative influence of chemical shrinkage on the higher basic shrinkage observed for AAS.

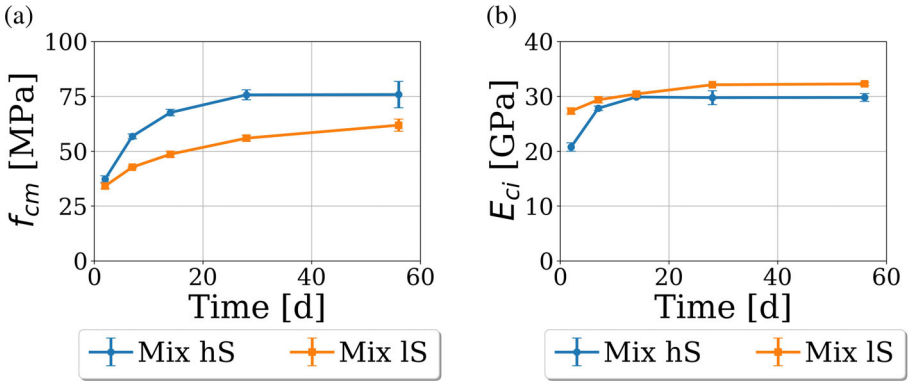

FIGURE 1 Strength development of both mixes. Compressive strength (a); Young's modulus (b). The error bars correspond to the standard deviation done on six samples

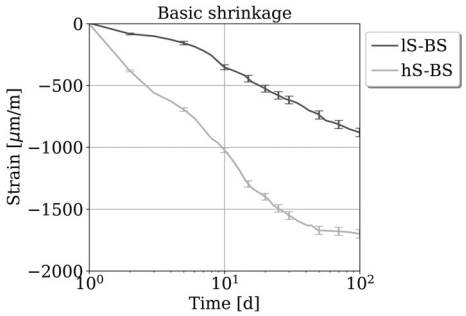

FIGURE 2 Basic shrinkage of both mixes lS and hS

The influence of the bulk modulus and the degree of saturation were discussed on one hand by Di Bella et al.[68] for cementitious systems and on the other hand by Ye et al. for AAS systems.[61] They all agree on the secondary influence of the bulk modulus. However, Di Bella et al.[68] consider that the degree of saturation plays a crucial role on the shrinkage performance, while Ye et al.[61] consider that its influence is quite low.

Basic shrinkage also depends on the drop in internal relative humidity RH_i due to consumption of water during the reaction. For AAS, RH_i is measured at 82%–83%[40,69] or even at 80%[8] and 75%.[31] In comparison, Jensen & Hensen[70] obtained RH_i higher than 80% after 1 year for different water-to-cement ratio for OPC systems with silica fume addition from 0% to 30%. Lura et al.[27] measured a RH_i of 92% after 7 days for OPC. Higher drop in RH_i for AAS can be attributed to more consumption of water during the activation and to the increased presence of alkali ions in pore solution resulting in lower RH in accordance to Raoult's law. The higher drop of relative humidity for AAS systems increases the capillary pressure and can explain the higher shrinkage observed.[31,40,69]

4.1.3 | Drying shrinkage

The Figure 3 shows the experimental results from the present study for drying shrinkage at RH = 65%. The results indicate the predominance of the exposure age. For the mix lS, the total shrinkage is 1289, 975, and 940 μm/m for the samples lS-DS-1d, ls-DS-7d, and ls-DS-28d, respectively, at age 100 days, that is, at drying age of 99, 93, and 72 days, respectively. Correspondingly, the drying shrinkage is 410, 96, and 61 μm/m for the samples lS-DS-1d, ls-DS-7d, and ls-DS-28d, respectively. For the mix hS, after 100 days, the total shrinkage is 3019, 1873, and 1756 μm/m for the samples hS-DS-1d, hS-DS-7d, and hS-DS-28d. This corresponds to a drying shrinkage of 1319, 173, and 56 μm/m for the samples hS-DS-1d, hs-DS-7d, and hs-DS-28d, respectively. Thus, covering the specimens during the first day is necessary for practical applications to reduce drying shrinkage.

The contribution of drying shrinkage to that of overall shrinkage is found to be relatively low for experiments on AAS concretes. For the mix lS, the drying shrinkage is responsible for 31.8%, 9.8%, and 6.4% of the total shrinkage at 100 days for exposure ages of 1, 7, and 28 days, respectively. For the mix hS, the drying shrinkage is responsible for 43.7%, 9.2%, and 3.2% of the total shrinkage at 100 days for exposure ages of 1, 7, and 28 days, respectively.

The results of shrinkage measurements and mass change depending on the ambient relative humidity (43% RH, 65% RH, and 85% RH) for the mix lS with an exposure age of 7 days are given in Figure 4. The mass change is defined as:

$$\Delta M(t) = \frac{M(t)}{M(t = t_s)} * 100 \tag{18}$$

The specimen lS-DS-RH-43% induces a shrinkage as high as for the specimen ls-DS-7d, despite a higher mass loss. As for waterglass-activated slag mortars,[29] lower ambient relative humidity implies higher drying shrinkage. There is the same threshold at relative humidity (between RH = 43% and RH = 65%) as reported by Ye et al.[29]

The specimen lS-DS-RH-85% shrinks less than the specimen under sealed conditions and its mass grows

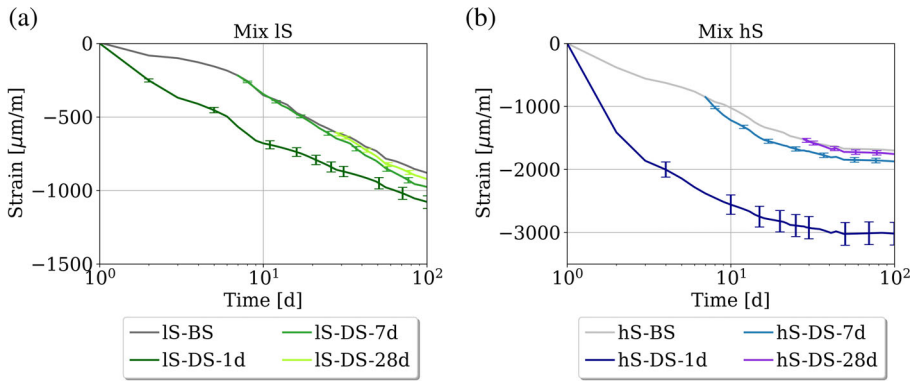

FIGURE 3 Total shrinkage of (a) mix lS and (b) mix hS with different age of exposure to drying. Total shrinkage is defined as the sum of basic shrinkage (under sealed condition) and drying shrinkage

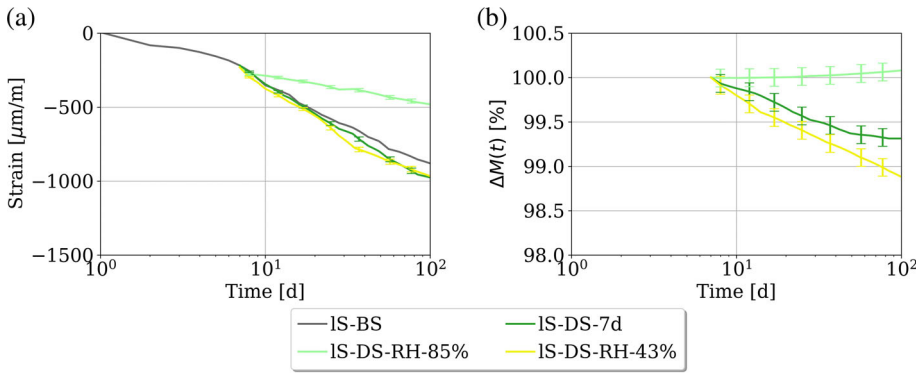

FIGURE 4 Drying shrinkage: Influence of the relative humidity on the mix lS. (a): Shrinkage, (b) mass

with time. As discussed above for the basic shrinkage, the drop of relative humidity in AAS concrete is higher than for cement-based concrete. Thus, when the specimens are exposed to drying, after 7 or 28 days, the imposed RH gradient is low in comparison to OPC-based concrete. The increase in mass after exposure for the specimens lS-DS-RH-85% indicates that the internal relative humidity of the mix lS after 7 days is below 85%, in accordance with Li et al.[8] or Li et al.[31]

4.2 | Calibration of the *fib* MC 2010 for strength and shrinkage on experimental results of AAS

4.2.1 | Type of concrete

As explained in Section 3, shrinkage models in the *fib* MC 2010 distinguish three types of concrete depending on the strength class of cement. Hence it is essential to first define the equivalent strength classes for the two AAS concrete mixes studied experimentally. This equivalent class is obtained by calibrating the model for strength development with experimental data on the coefficient s in Equations (2) and (4). The optimized values of s for both mixes tested are given in Table 6. Based on this calibration and on the compressive strength given in Table 2, the equivalent strength class for both mixes is the class of cements 42.5 R, 52.5 N, 52.5 R, or superior. Thus, the AAS concrete is considered to be equivalent to these types of concrete as defined in the *fib* MC 2010.

TABLE 6 Optimization of the coefficient s for alkali activated slag with waterglass

Mix	*s* following (2)	*s* following (4)
Mix lS	0.21	0.13
Mix hS	0.26	0.23

4.2.2 | Calibration of basic shrinkage experiments

The Figure 5 shows the comparison between the results from this study, the experimental results for three different studies obtained from the literature[55,62,71] and the predictions with the models from the *fib* MC 2010, which are applicable for OPC concrete. The shrinkage results are expressed in terms of the normalized shrinkage $\frac{\varepsilon_{cbs}}{\varepsilon_{cbs0}}$ to have a consistent comparison between different mixes, independently from the compressive strength f_{cm}. Indeed, for the *fib* MC 2010, the ratio $\frac{\varepsilon_{cbs}}{\varepsilon_{cbs0}} = \beta_{bs}(t)$ ranges from 0 to 1. However, as mentioned above and shown in

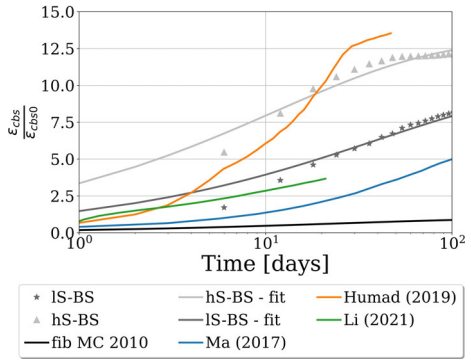

FIGURE 5 Comparison of basic shrinkage results with literature results and the fib MC 2010 prediction. Comparison performed on the ratio ξ_{cbs}/ξ_{cbs0}. Calibration of the curve following the equations (14) and (15)

TABLE 7 Obtained parameters for basic shrinkage extension of the *fib* MC 2010

Specimens	$\xi_{cbs,1}$	$\xi_{cbs,2}$
lS-BS	9.90	0.80
hS-BS	13.0	1.51

Figure 5 the final shrinkage for AAS is much more than that for OPC concrete. The obtained results for both lS and hS mixes with the extension of the *fib* MC 2010 given by Equation (14) are also shown in Figure 5 and correspondingly, the calibrated parameters are given in Table 7. The obtained values for $\xi_{cbs,2}$ indicate that the speed of shrinkage of AAS systems is comparable to the one from the *fib* MC 2010. In accordance to what can be found in the literature,[55,62,71] the final basic shrinkage of AAS concrete, characterized by the value $\xi_{cbs,1}$, is much higher than the final basic shrinkage of OPC-based concrete. In terms of mechanisms, this could be due to the lower relative humidity measured in AAS systems.[8,31,40,69]

4.2.3 | Calibration of drying shrinkage experiments

For drying shrinkage, the predictions using the model from the *fib* MC 2010 and the extension proposed in this study as given by Equation (16) are shown in Figure 6. The calibrated coefficients corresponding to the model extension are provided in Table 8.

As explained in Section 4.1.3, the age of exposure to drying plays an important role on final drying shrinkage for AAS concrete. However, it is not captured by the original *fib* MC 2010. For the strength class f_{cm} (chosen between 56 and 76 MPa) and for exposure ages between

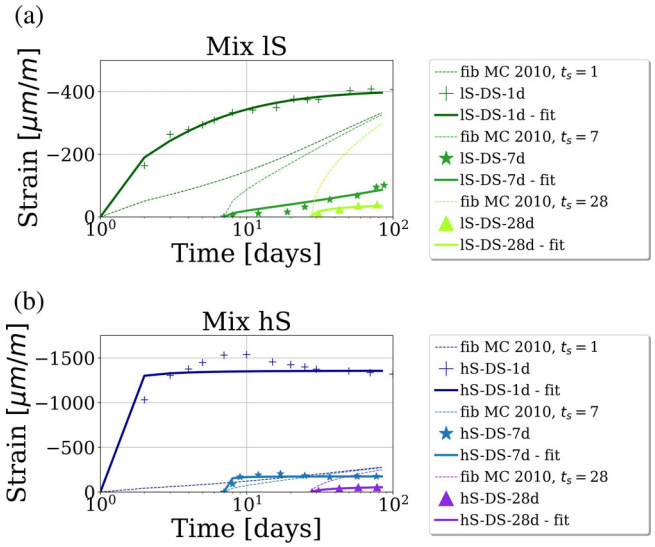

FIGURE 6 Experimental results of drying shrinkage for (a) mix lS (b) mix hS. Dashed lines correspond to the prediction from the fib MC 2010. Plain lines correspond to the adapted model

TABLE 8 Obtained parameters for drying shrinkage extension of the *fib* MC 2010

Specimens	$\xi_{cds,1}$	$\xi_{cds,2}$
lS-DS-1d	8.5×10^{-1}	4.1×10^{-2}
lS-DS-7d	3.6×10^{-1}	2.6
lS-DS-28d	8.3×10^{-2}	1.7×10^{-1}
hS-DS-1d	3.5	2.0×10^{-3}
hS-DS-7d	4.4×10^{-1}	3.3×10^{-3}
hS-DS-28d	1.6×10^{-1}	3.2×10^{-1}

1 and 28 days, the drying shrinkage after 100 days ε_{cds} as predicted by the model from the *fib* MC 2010 is in the range of 248 and 352 μm/m. The specimen lS-DS-1d is the only one with this order of magnitude, whereas hS-DS-1d is largely underestimated. On the other hand, the specimens with later exposure (7 or 28 days) are largely overestimated. This explains why the obtained coefficients $\xi_{cds,1}$ for the proposed model extension decrease with exposure age for each mix. It can also be noted that $\xi_{cds,1}$ is higher than 1, only for the specimen hS-DS-1d, which implies that the absolute value of drying shrinkage of AAS concrete is quite overestimated in the *fib* MC 2010.

Moreover, the relative importance of drying shrinkage when compared with basic shrinkage is overestimated by models from the *fib* MC 2010. These models predict that the drying shrinkage is responsible for more than 70% of the total shrinkage, which is much higher than that reported in this study for AAS concrete (see Section 4.1.3). In addition, the optimized values of $\xi_{cds,2}$ are lower than

1, indicating that the drying shrinkage occurs faster for AAS concrete than OPC concrete. This is especially true for specimens exposed at early age, namely, lS-DS-1d, and hS-DS-1d. This result is in agreement with what can be found in literature.[62,71]

For the specimen lS-DS-RH-85%, the shrinkage is lower than the one of lS-BS (under sealed conditions). This is due to the fact that the RH_i of the samples is less than ambient RH under exposure at 85%. In this last environment condition, there is even an increase in RH_i of the sample and it results consequently expansive strains. This indicates that the bounds of applicability in Equation (11) must be adjusted for AAS concrete from 40%–99% β_{s1} to at least 40%–85% β_{s1}.

5 | APPLICATION OF THE EXTENSION AND VALIDATION

To evaluate the potential relevance of the model extension given by Equations (14), (15), and (16), the four coefficients $\xi_{cbs,1}$, $\xi_{cbs,2}$, $\xi_{cds,1}$, and $\xi_{cds,2}$ are obtained using the results from the present study. Finally, using these defined parameters, the model for total shrinkage is compared with experimental results from the literature to validate it.

5.1 | Calibrated parameters for model extension

Basic shrinkage results of the calibration, given in Table 7, show the importance of the parameter M_S, which is in accordance with Ballekere Kumarappa et al. and Atis et al.[30,58] To account for this, a linear correlation is proposed between $\xi_{cbs,1}$ and M_S. Results on mortars[30] indicate that the alkalinity coefficient n has an equivalent influence on the basic shrinkage. However, due to lack of data on concrete level, for the present study this parameter is not taken into account. The speed of shrinkage, characterized by the coefficient $\xi_{cbs,2}$, is also modeled with a linear curve, from both results lS-BS and hS-BS. Since both calibrations are derived from only two data points, future results of basic shrinkage of AAS with different M_S should help to refine these correlations. Thus the parameters for the extended *fib* model for basic shrinkage can be taken as follows:

$$\begin{cases} \xi_{cbs,1}(M_S) &= 1.83 \cdot M_S + 8.98 \\ \xi_{cbs,2}(M_S) &= 0.41 \cdot M_S + 0.59 \end{cases} \quad (19)$$

For drying shrinkage, the exposure age to drying (t_s) influences greatly the final drying shrinkage. The influence at early-age (1 to 7 days) seems to be greater than that at later ages. Indeed, the activation of slag with sodium-silicate is slower than the hydration of cement and the second acceleration period can occur up to 48 h.[46] Thus, the material behavior is more sensitive to any water loss at early age. For this reason, the calibration of the coefficients in the extended model split into two domains [1, 7] days and [7, 28] days. Between 1 and 7 days, a decreasing exponential model is used, while a linear curve is used between 7 and 28 days. For $\xi_{cds,2}$, the experimental results indicate that lower the t_s, the faster is the drying shrinkage. However, there was a large range of variation of the obtained $\xi_{cds,2}$ up to third order of magnitude (10^{-3}–10^{0}). In comparison with the range of data available from the literature, it was found that fixing $\xi_{cds,2}$ to 0.25 is a good approximation. The value 0.25 also corresponds to the average value of $\xi_{cds,2}$ for the drying shrinkage with exposure after 28 days for mixes lS and hS. Thus, the key parameters for extended *fib* model for drying shrinkage are as below:

$$\begin{cases} \xi_{cds,1}(1 \le t_s \le 7) &= 7.9 \cdot \exp\left(-\left(\frac{t_s}{1.6}\right)^{2.5}\right) + 0.40 \\ \xi_{cds,1}(t_s > 7) &= -1.3 \cdot 10^{-2} \cdot t_S + 4.91 \cdot 10^{-1} \\ \xi_{cds,2}(t_s) &= 0.25 \end{cases} \quad (20)$$

Finally, it is emphasized that the parameters and correlations provided above are based on the limited dataset of the present study. Thus, a future recalibration will be needed on a larger dataset before using the model for practical engineering purposes. In particular, the influence of slag composition on shrinkage should be investigated with the use of either the ratio $\frac{CaO}{SiO_2+Al_2O_3}$ proposed by Chen et al.[26] for SCM or the ratio $\frac{CaO+MgO}{SiO_2}$ that has been used for correlations on degree of reaction of AAS.[47,48]

5.2 | Validation on results from the literature

The proposed extension is validated against the shrinkage results from Ma et al.,[62] Taghvayi et al.,[63] and Humad et al.[71] For the results from Ma et al. and Humad et al., as both total shrinkage and basic shrinkage are distinguished, the model results are also plotted in a distinguished manner. For each mix, all the necessary parameters for the extended model were taken from the papers. The input parameters for models comprises of compressive strength, drying age, notional thickness, relative humidity, and silicate ratio (M_S). The equivalent binder type was determined using the compressive

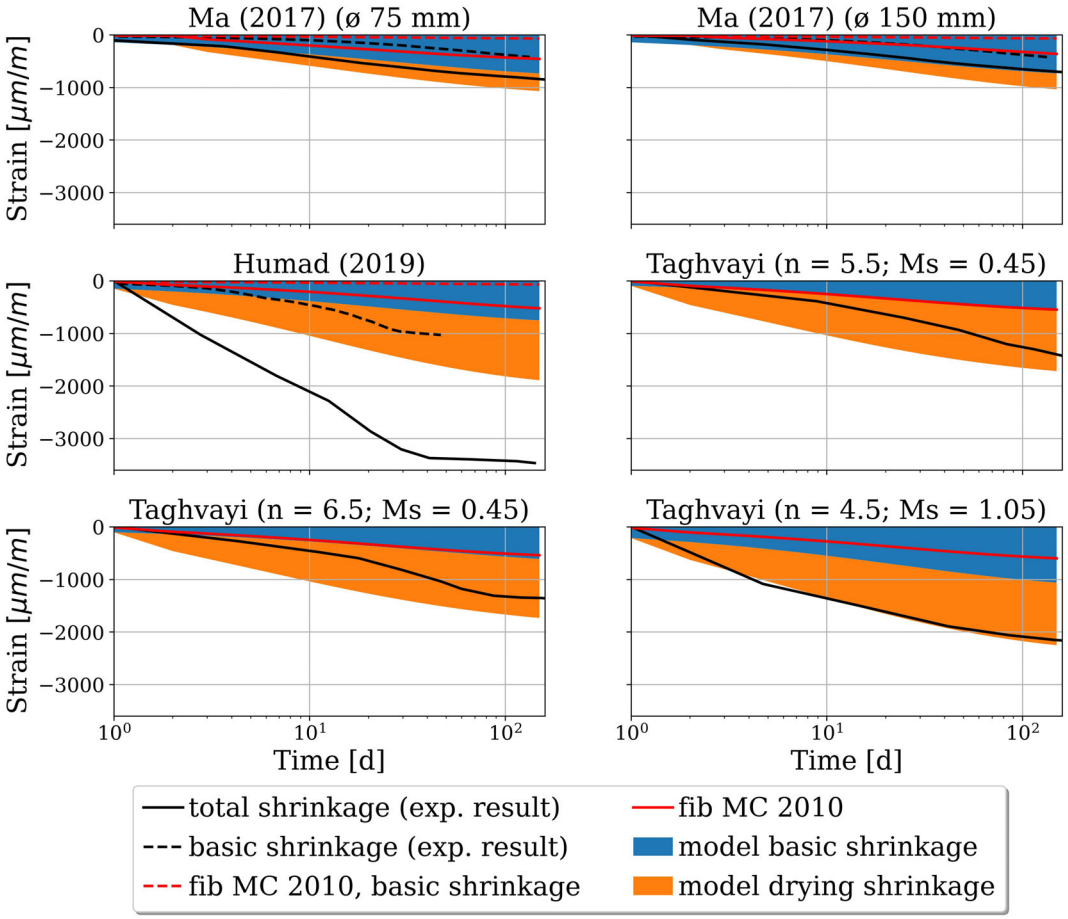

FIGURE 7 Prediction of total shrinkage for dataset extracted from literature (a) Ma et al. (2018) (ø 150 mm), (b) Ma et al. (2018) (ø 150 mm), (c) Humad et al. (2019), (d) Taghvayi et al. (2018) (with $n = 5.5$ and Ms = 0.45), (e) Taghvayi et al. (2018) (with $n = 6.5$ and Ms = 0.45), and (f) Taghvayi et al. (2018) (with $n = 4.5$ and Ms = 1.05)

strength development as shown in Section 4.2.1. The obtained s was approximated to the closest coefficient from Table 4. These inputs are provided in Supporting Information.

The results for shrinkage predictions are given in Figure 7. Since the results from Taghvayi et al.[63] comprise of 20 experiments, only three results are presented here as examples. Additional results can be found in Supporting Information. The basic shrinkage from Ma et al.[62] is overestimated, but the drying shrinkage for both radius 75 and 150 mm are well predicted. In the study done by Humad et al.,[71] the prediction underestimates both basic shrinkage and drying shrinkage but provides significantly better results than models from the *fib* MC 2010. This dataset comes from the blending of a slag with 30.4% CaO, 35% SiO_2, 14.3% Al_2O_3, and 16.1% MgO, with an alkali solution of water/binder ratio equal to 0.36, a sodium silicate content of 5% of mass, and MS equal to 1. One can note that the MgO content is quite high in comparison with the slags from Li et al.[31] and Taghvayi et al.[63] or from the present study. Taghvayi et al.[63] do not distinguish basic shrinkage and drying shrinkage. Thus, only the total shrinkage is analyzed. In all the tested mixes, the prediction using the extended models significantly improves the predictions when compared with the models from *fib* MC 2010.

6 | CONCLUSION

In this study, new experimental results of both basic and drying shrinkage have been presented for AAS concrete. Basic shrinkage is much higher for AAS concrete than for OPC concrete. Furthermore, the basic shrinkage increases with higher M_S. The drying shrinkage is very dependent on the exposure age to drying t_s.

The extended models of the *fib* MC 2010 proposed in this study have been calibrated based on the performed experiments. The four parameters ξ_{cbs1}, ξ_{cds1}, ξ_{cbs2}, and ξ_{cds2} in the model extension influence the final values of basic shrinkage and drying shrinkage and the speed of basic shrinkage and drying shrinkage, respectively. ξ_{cbs1} increases with M_S and is found to be higher than 1, indicating a higher final basic shrinkage when compared with OPC concrete. Higher M_S leads to faster basic

shrinkage. The drying shrinkage is very high for an exposure to drying in early ages and ξ_{cds1} is modeled as a decreasing exponential function during first 7 days. ξ_{cds2} is found to be lower than 1 indicating that the speed of drying shrinkage is faster than the one predicted in the original models from *fib* MC 2010. The calibrated extended model on experimental data presented in this study significantly improves the prediction when compared with the original *fib* MC 2010 for both basic and drying shrinkage on validation datasets taken from the literature. Further calibration is needed on larger datasets to improve the model predictions varying different parameters affecting AAS concrete mixes such as n or the MgO content of the slag.

ACKNOWLEDGMENT

The project leading to this application has received funding from the European Union's Horizon 2020 research and innovation programme under the Marie Skłodowska–Curie grant agreement No. 813596.

CONFLICT OF INTEREST

The authors declare that they have no conflict of interest.

DATA AVAILABILITY STATEMENT

The data that support the findings of this study are available from the corresponding author upon reasonable request.

ORCID

Richard Caron https://orcid.org/0000-0002-5741-6440

REFERENCES

1. Fernández-Jiménez A, Puertas F. Structure of calcium silicate hydrates formed in alkaline-activated slag: influence of the type of alkaline activator. J Am Ceram Soc. 2003;86:1389–94.
2. Komljenović MM, Baščarević Z, Marjanović N, Nikolić V. Decalcification resistance of alkali-activated slag. J Hazard Mater. 2012;233–234:112–21.
3. Komljenović M, Baščarević Z, Marjanović N, Nikolić V. External sulfate attack on alkali-activated slag. Construct Build Mater. 2013;49(7):31–9.
4. Chang JJ. A study on the setting characteristics of sodium silicate-activated slag pastes. Cem Concr Res. 2003;33(7):1005–11.
5. Jansson H, Tang L. Parameters influencing the initial setting time of alkali-activated ground granulated blastfurnace slag materials. the nordic concrete federation, 2005.
6. Bakharev T, Sanjayan JG, Cheng YB. Resistance of alkali-activated slag concrete to carbonation. Cem Concr Res. 2001; 31:1277–83.
7. Cadore DE, Angulski da Luz C, Farias de Medeiros MH. An investigation of the carbonation of alkaline activated cement made from blast furnace slag generated by charcoal. Construct Build Mater. 2019;226:117–25.
8. Li Z, Liu J, Ye G. Drying shrinkage of alkali-activated slag and fly ash concrete; a comparative study with ordinary Portland cement concrete. Heron. 2019;64:106107.
9. Thomas RJ, Peethamparan S. Alkali-activated concrete: engineering properties and stress–strain behavior. Construct Build Mater. 2015;93(4):49–56.
10. Collins F, Sanjayan JG. Effect of pore size distribution on drying shrinkage of alkali-activated slag concrete. Cem Concr Res. 2000;30:1401–6.
11. Aili A, Vandamme M, Torrenti JM, Masson B. Is long-term autogenous shrinkage a creep phenomenon induced by capillary effects due to self-desiccation? Cem Concr Res. 2018;108(2):186–200.
12. Hossain AB, Weiss J. The role of specimen geometry and boundary conditions on stress development and cracking in the restrained ring test. Cem Concr Res. 2006;36(1):189–99.
13. Shah HR, Weiss J. Quantifying shrinkage cracking in fiber reinforced concrete using the ring test. Mater Struct. 2006; 39(9):887–99.
14. ACI Committee 209. 209R-92: Prediction of Creep, Shrinkage, and Temperature Effects in Concrete Structures (Reapproved 2008). Technical Documents.
15. Bazant ZP, Baweja S. Creep and shrinkage prediction model for analysis and design of concrete structures- model B_3. Mater Struct. 1995;28:357–65. 415–430, 488–495.
16. Bazant ZP, Baweja S. Creep and Shrinkage Prediction Model for Analysis and Design of Concrete Structures: Model B3. As submitted for: Adam Neville Symposium: Creep and Shrinkage—Structural Design Effects 2000; ACI SP-194, A.Al-Manaseer, ed., Am. Concrete Institute, Farmington Hills, MI: 1–83.
17. Gardner NJ. Design provisions for drying shrinkage and creep of Normal strength concrete. In: Al-Manaseer A, editor. The Adam Neville symposium: creep and shrinkage-structural design effects;SP-194. Farmington Hills, MI: American Concrete Institute; 2000. p. 101–34.
18. Muller HS, Hillsdorf HK. General task group 9. Paris, France: CEB Bomité Euro-Internaional du Béton; 1990. p. 201.
19. CEB. Evaluation of the Time Dependent Properties of Concrete. Bulletin d'Information 1991; No. 199 (Comité European du Beton/Federation Internationale de la Precontrainte, Lausanne, Switzerland, 1991, 201).
20. CEB. CEB-FIP Model Code 1990. CEB Bulletin d'Information 1993; No. 213/214 (Comité Euro-International du Béton, Lausanne, Switzerland), 1993, 33–41.
21. CEB. Structural Concrete—Textbook on Behaviour, Design and Performance. Updated Knowledge of the CEB/FIP Model Code 1990. fib Bulletin 1999;2 V.2(Federation Internationale du Beton, Lausanne, Switzerland), 1990, 37–52.
22. FIB. fib model code for concrete structures 2010. Lausanne: International Federation for Structural Concrete (fib); 2013.
23. Bažant ZP, Hubler MH, Wan-Wendner R. Model B4 for concrete creep and shrinkage including multi-decade applicability. RILEM Mater Struct. 2015;01(48):753–70.
24. Hubler MH, Wendner R, Baant ZP. Comprehensive database for concrete creep and shrinkage: analysis and recommendations for testing and recording. ACI Mater J. 2015;112: 547–58.
25. Tošić N, de La Fuente A, Marinković S. Shrinkage of recycled aggregate concrete: experimental database and application of fib model code 2010. Mater Struct. 2018;51(5):125.
26. Chen J, Kuder KG, Lehman DE, Roeder CW, Lowes LN. Creep modeling of concretes with high volumes of supplementary cementitious materials and its application to concrete-filled tubes. Mater Struct. 2017;50(1):139.

27. Lura P, Jensen OM, van Breugel K. Autogenous shrinkage in high-performance cement paste: an evaluation of basic mechanisms. Cem Concr Res. 2003;33:223–32.
28. Jensen OM. Autogenous deformation and RH-change in perspective. Cem Concr Res. 2001;31:1859–65.
29. Ye H, Cartwright C, Rajabipour F, Radlińska A. Understanding the drying shrinkage performance of alkali-activated slag mortars. Cem Concr Compos. 2017;76(1):13–24.
30. Ballekere Kumarappa D, Peethamparan S, Ngami M. Autogenous shrinkage of alkali activated slag mortars: basic mechanisms and mitigation methods. Cem Concr Res. 2018;109(3):1–9.
31. Li Z, Lu T, Liang X, Dong H, Ye G. Mechanisms of autogenous shrinkage of alkali-activated slag and fly ash pastes. Cem Concr Res. 2020;135:106107.
32. Bangham DH, Fakhoury N, Mohamed AF. The swelling of charcoal. Part II. Some factors controlling the expansion caused by water, benzene and pyridine Vapours. Proc R Soc Lond. 1932;138(834):162–183.
33. Hiller KH. Strength reduction and length changes in porous glass caused by water vapor adsorption. J Appl Phys. 1964; 35(5):1622–8.
34. Feldman RF, Serada PJ. A new model for hydrated Portland cement and its practical implications. NRC of Canada. 1970;53:53–9.
35. Wittmann FH. Creep and shrinkage mechanisms. In: Bazant ZP, Wittmann FH, editors. Part II in "Creep and shrinkage in concrete structures". Chichester: John Wiley & Sons; 1982. p. 129–63.
36. Churaev NV, Derjaguin BV. Inclusion of structural forces in the theory of stability of colloids and films. J Colloid Interface Sci. 1985;103(2):542–53.
37. Wittmann FH, Beltzung F. Fundamental aspects of the interaction between hardened cement paste and water applied to improve prediction of shrinkage and creep of concrete: a critical review. J Sustain Cem-Based Mater. 2016;5(1–2):106–16.
38. Lu T, Li Z, van Breugel K. Modelling of autogenous shrinkage of hardening cement paste. Construct Build Mater. 2020; 264(15):120708.
39. Melo Neto AA, Cincotto MA, Repette W. Drying and autogenous shrinkage of pastes and mortars with activated slag cement. Cem Concr Res. 2008;38(4):565–74.
40. Song C, Choi YC, Choi S. Effect of internal curing by superabsorbent polymers—internal relative humidity and autogenous shrinkage of alkali-activated slag mortars. Construct Build Mater. 2016;123(10):198–206.
41. Mastali M, Kinnunen P, Dalvand A, Mohammadi Firouz R, Illikainen M. Drying shrinkage in alkali-activated binders—a critical review. Construct Build Mater. 2018;190(8):533–50.
42. Bernal SA, San Nicolas R, van Deventer JSV, Provis JL. Water content modifies the structural development of sodium metasilicate-activated slag binders. Revista ALCONPAT. 2015; 5(1):28–39.
43. Criado M, Walkley B, Ke X, Provis J, Bernal S. Slag and activator chemistry control the reaction kinetics of sodium Metasilicate-activated slag cements. Sustainability. 2018;10(12):4709.
44. Zuo Y, Ye G. Preliminary interpretation of the induction period in hydration of sodium hydroxide/silicate activated slag. Materials. 2020;13(21):4796.
45. Chithiraputhiran S, Neithalath N. Isothermal reaction kinetics and temperature dependence of alkali activation of slag, fly ash and their blends. Construct Build Mater. 2013;45:233–42.
46. Gebregziabiher BS, Thomas RJ, Peethamparan S. Temperature and activator effect on early-age reaction kinetics of alkali-activated slag binders. Construct Build Mater. 2016;113(1): 783–93.
47. Winnefeld F, Ben Haha M, Le Saout G, Costoya M, Ko SC, Lothenbach B. Influence of slag composition on the hydration of alkali-activated slags. J Sustain Cem-Based Mater. 2015;4(2): 85–100.
48. Caron R, Patel RA, Dehn F. Activation kinetic model and mechanisms for alkali-activated slag cements. Construct Build Mater. 2022;323:126577.
49. DIN EN 12350-5. Prüfung von Frischbeton—Teil 5: Ausbreitmaß; Deutsche Fassung EN 12350-5:2019. Beuth Verlag 2019;.
50. DIN EN 12350-6. Prüfung von Frischbeton—Teil 6: Frischbetonrohdichte; Deutsche Fassung EN 12350-6:2019. Beuth Verlag 2019.
51. DIN EN 12350-7. Prüfung von Frischbeton—Teil 7: Luftgehalt – Druckverfahren; Deutsche Fassung EN 12350-7:2019. Beuth Verlag 2019.
52. DIN EN 12390-3. Prüfung von Festbeton—Teil 3: Druckfestigkeit von Probekörpern; Deutsche Fassung EN 12390-3:2019. Beuth Verlag 2019.
53. DIN EN 12390-13. Prüfung von Festbeton—Teil 13: Bestimmung des Elastizitätsmoduls unter Druckbelastung(Sekantenmodul); Deutsche und Englische Fassung prEN 12390-13:2019. Beuth Verlag 2019.
54. DIN EN 12390-16. Prüfung von Festbeton - Teil 16: Bestimmung des Schwindens von Beton; Deutsche Fassung EN 12390-16:2019. Beuth Verlag 2019;.
55. Li Z, Lu T, Chen Y, Wu B, Ye G. Prediction of the autogenous shrinkage and microcracking of alkali-activated slag and fly ash concrete. Cem Concr Compos. 2021;117:103913.
56. Palacios M, Puertas F. Effect of shrinkage-reducing admixtures on the properties of alkali-activated slag mortars and pastes. Cem Concr Res. 2007;37(5):691–702.
57. Cartwright C, Rajabipour F, Radlińska A. Shrinkage characteristics of alkali-activated slag cements. J Mater Civ Eng. 2015; 27(7):509.
58. Duran Atiş C, Bilim C, Çelik Ö, Karahan O. Influence of activator on the strength and drying shrinkage of alkali-activated slag mortar. Construct Build Mater. 2009;23(1):548–55.
59. Aydn S, Baradan B. Mechanical and microstructural properties of heat cured alkali-activated slag mortars. Mater Design. 2012; 35:374–83.
60. Matalkah F, Salem T, Shaafaey M, Soroushian P. Drying shrinkage of alkali activated binders cured at room temperature. Construct Build Mater. 2019;201(1):563–70.
61. Ye H, Cartwright C, Rajabipour F, Radlinska A. Effect of Drying Rate on Shrinkage of Alkali-Activated Slag Cements 2014.
62. Ma J, Dehn F. Shrinkage and creep behavior of an alkali-activated slag concrete. Struct Concr. 2017;18(5):801–10.
63. Taghvayi H, Behfarnia K, Khalili M. The effect of alkali concentration and sodium silicate modulus on the properties of alkali-activated slag concrete. J Adv Concrete Technol. 2018; 16(7):293–305.
64. Cartwright C, Rajabipour F, Radlinska A. Measuring the chemical shrinkage of alkali-activated slag cements using the Buoyancy Method. Ninth International Conference on Creep, Shrinkage, and Durability Mechanics (CONCREEP-9), 2013;308–15.
65. Ye H, Radlińska A. Quantitative analysis of phase assemblage and chemical shrinkage of alkali-activated slag. J Adv Concrete Technol. 2016;14(5):245–60.

66. Thomas JJ, Allen AJ, Jennings HM. Density and water content of nanoscale solid C–S–H formed in alkali-activated slag (AAS) paste and implications for chemical shrinkage. Cem Concr Res. 2012;42(2):377–83.
67. Zhang T, Gao P, Luo R, Guo Y, Wei J, Yu Q. Measurement of chemical shrinkage of cement paste: comparison study of ASTM C 1608 and an improved method. Construct Build Mater. 2013;48(2):662–9.
68. Di Bella C, Wyrzykowski M, Lura P. Evaluation of the ultimate drying shrinkage of cement-based mortars with poroelastic models. Mater Struct. 2017;50(1):453.
69. Jia Z, Yang Y, Yang L, Zhang Y, Sun Z. Hydration products, internal relative humidity and drying shrinkage of alkali activated slag mortar with expansion agents. Construct Build Mater. 2018;158(2):198–207.
70. Jensen OM, Hansen PF. Autogenous relative humidity change in silica fume-modified cement paste. Adv Cem Res. 1995; 7(25):33–8.
71. Humad AM, Kothari A, Provis JL, Cwirzen A. The effect of blast furnace slag/Fly ash ratio on setting, strength, and shrinkage of alkali-activated pastes and concretes. Front Mater. 2019;6:113.

AUTHOR BIOGRAPHIES

Richard Caron, Institute of Building Materials and Concrete Structures (IMB), Karlsruhe Institute of Technology (KIT), Germany.
Email: richard.caron@kit.edu

Ravi A. Patel, Materials Testing and Research Institute (MPA), Karlsruhe Institute of Technology (KIT), Germany
Email: ravi.patel@kit.edu

Frank Dehn, Institute of Building Materials and Concrete Structures (IMB), Karlsruhe Institute of Technology (KIT), Germany
Email: frank.dehn@kit.edu

SUPPORTING INFORMATION

Additional supporting information may be found in the online version of the article at the publisher's website.

How to cite this article: Caron R, Patel RA, Dehn F. Extension of the *fib* MC 2010 for basic and drying shrinkage of alkali-activated slag concretes. Structural Concrete. 2022. https://doi.org/10.1002/suco.202100901